Materials Today Communications 33 (2022) 104461

Contents lists available at ScienceDirect

Materials Today Communications

journal homepage: www.elsevier.com/locate/mtcomm

FAI: Fast, accurate, and intelligent approach and prediction tool for flexural capacity of FRP-RC beams based on super-learner machine learning model

Tadesse G. Wakjira, Abdelrahman Abushanab, Usama Ebead, Wael Alnahhal *

Department of Civil and Architectural Engineering, College of Engineering, Qatar University, P.O. Box 2713, Doha, Qatar

ARTICLE INFO

Keywords:
FRP bars
Flexural
Machine learning
Super-Learner
Design
Prediction tool

ABSTRACT

Fiber-reinforced polymer (FRP) composites have recently been considered in the field of structural engineering as one of the best alternatives to conventional steel reinforcement due to their high tensile strength, lightweight, cost-effectiveness, and superior corrosion resistance. However, the variation in FRP physical and mechanical characteristics among the different FRP types and manufacturers makes it difficult to predict the strength of FRP-reinforced concrete (RC) members. For that reason, an efficient prediction tool was developed for a fast, accurate, and intelligent (FAI) prediction of the flexural capacity of FRP-RC beams based on the result of an optimized super-learner machine learning (ML) model. A database of the experimental results on the flexural strength of FRP-RC beams was compiled and randomly split into 80% train and 20% test sets. Six factors were considered in the model; namely, width and effective depth of the beam, concrete compressive strength, FRP flexural reinforcement ratio, FRP modulus of elasticity, and FRP ultimate tensile strength. Grid search is combined with a 10-fold cross-validation to optimize the hyperparameters of the ML models. The prediction capability of the proposed super-learner ML model was benchmarked against boosting- and tree-based ML models, such as classification and regression trees, adaptive boosting, gradient boosted decision trees, and extreme gradient boosting. Moreover, a comparison with the existing code and guideline equations showed that the proposed super-learner ML model provided the most desirable prediction of the flexural capacity of FRP-RC beams.

1. Introduction

Steel corrosion is a universal concern that poses significant risks and challenges to reinforced concrete (RC) structures, especially those exposed to aggressive environments. One out of every seven bridges in the United States undergoes significant steel corrosion, and about USD 4 billion is expended annually to maintain and repair their corrosion-damaged elements [1,2]. The latter is not only costly but also reduces the serviceability of such structures and disturbs the public through road and building closures during the repair work, which can cost 10 times the corrosion repair itself [2]. This has prompted researchers to investigate the feasibility of replacing conventional steel reinforcement with non-corrosive reinforcement. In this context, fiber-reinforced polymer (FRP) composites have been highlighted as durable reinforcement for RC structures due to their high tensile strength, lightweight, cost-effectiveness, and non-corrosiveness compared with conventional steel reinforcement [3]. Despite the beneficial properties of FRP reinforcement, its widespread use applications is restricted due to its brittleness, low elastic modulus, and high initial cost [3]. Thus, numerous studies evaluated the structural performance of RC members with various types of FRP composites, including glass FRP (GFRP), carbon FRP (CFRP), aramid FRP (AFRP), and basalt (BFRP) to ensure the safety and serviceability of such members and to establish comprehensive design guidelines for broader FRP-RC applications [4–9].

The flexural behavior of FRP-RC beams has been extensively investigated [4,5,10–13]. Adam et al. [4] investigated the flexural behavior of RC beams with GFRP bars and found that the crack widths and deflections were significantly decreased with an increase in the reinforcement ratio. In addition, the ultimate load was increased by 97% when the reinforcement ratio increased by 2.7 times the balanced reinforcement ratio. Abdelkarim et al. [10] evaluated the flexural behavior of GFRP-RC beams prepared with normal- and high-strength concrete. They observed that the reinforcement ratio and bar spacing were more influential on the beam service moment than the moment resistance. They also found that the beams recorded a higher moment resistance and ductility by increasing the compressive strength of concrete. In the study by Karayannis et al. [5], the failure mode of CFRP-RC beams is switched to shear as the reinforcement ratio increased. Ruan

* Corresponding author.
E-mail address: wael.alnahhal@qu.edu.qa (W. Alnahhal).

https://doi.org/10.1016/j.mtcomm.2022.104461
Received 24 July 2022; Received in revised form 2 September 2022; Accepted 13 September 2022
Available online 14 September 2022

et al. [11] noticed that hybrid steel-GFRP RC beams exhibited a slightly lower flexural capacity and showed deflections 1.15–2.1 times higher than those of steel-RC beams. In the work of Al-Rousan et al. [12], increasing the FRP reinforcement ratio from 0.38% to 0.46% and 0.57% increased the ultimate load by 7.3% and 17.1%, respectively.

Despite the ample research on the flexural behavior of FRP-RC beams, researchers have raised major concerns about the brittleness of FRP reinforcement and the consequent sudden failure and low ductility of FRP-RC members [3]. As a result, FRP design guidelines recommend overdesigning FRP-RC members to ensure that concrete crushing precedes FRP bar rupture, which allows for a higher deformability and progressive failure before full structural collapse [14–17]. Over-reinforced FRP-RC members are also preferred over under-reinforced members because of their high axial stiffness, which decreases their service crack width and deflection [6]. Meanwhile, the empirically analytical equations to predict the performance of FRP-RC members were established using limited experimental data on GFRP, CFRP, and AFRP-RC beams only. In addition, the existing FRP-RC guidelines do not account for BFRP-RC members [14–17]. Therefore, further research on the flexural capacity prediction of FRP-RC members is required to develop a comprehensive flexural model for all types of FRP composites.

Recently, with the development of artificial intelligence and computational capabilities, machine learning (ML) techniques have gained considerable attention in the field of structural engineering. Numerous classification and regression-based ML models have been developed to predict the failure mode and load capacity of RC columns and walls [18–22], shear capacity of concrete beams [23–30], plastic hinge length and seismic response of RC bridges and buildings [31–36], and axial load capacity of short FRP-RC columns [37]. However, the literature lacks the implementation of ML models to analyze the flexural capacity of FRP-RC beams. Therefore, this study investigated the application of tree- and boosting-based algorithms and super-learner model for predicting the flexural capacity of FRP-RC beams. First, a comprehensive experimental database of FRP-RC beams with different geometries, FRP reinforcement types and ratios, and mechanical properties of concrete and FRP composites was collected. The compiled database was randomly split into the train and test sets comprising 80% and 20% of the total dataset, respectively. Different tree- and boosting-based algorithms were then trained on the train set and evaluated on the unseen (test) set. Grid search was combined with 10-fold cross-validation to tune the hyperparameters of the ML models. After that, the super-learner model combined the optimized ML models to produce a strong single model. In addition, the results of the proposed models were compared with the analytical guideline formulations. Finally, the super-learner model was deployed to a web-based application for user-friendly *FAI*: fast, accurate, and intelligent flexural capacity prediction of FRP-RC beams.

2. Review of the current design provisions

The predicted flexural capacities of FRP-RC beams based on the developed ML models and the analytical estimates of ACI 440.1R-15 [14] and CAN/CSA-S806–12 [16] were compared with the experimental results. A brief review of the ACI 440.1R-15 [14] and CAN/-CSA-S806–12 [16] provisions is provided below.

2.1. ACI 440.1R-15 [14]

As per ACI 440.1R-15 [14], the flexural capacity of over-reinforced FRP-RC beams can be calculated as given in Eqs. (1) to (4):

$$M_n = \rho_f f_f \left(1 - 0.59\frac{\rho_f f_f}{f_c^{'}}\right) bd^2 \tag{1}$$

$$\rho_f = \frac{A_f}{bd} \tag{2}$$

$$f_f = \left[\sqrt{\frac{(E_f\varepsilon_{cu})^2}{4} + \frac{0.85\beta_1 f_c^{'}}{\rho_f}E_f\varepsilon_{cu}} - 0.5E_f\varepsilon_{cu}\right] \le f_{fu} \tag{3}$$

$$\beta_1 = \begin{Bmatrix} 17 \le f_c^{'} \le 28, \& \quad \beta_1 = 0.85 \\ 28 < f_c^{'} < 55, \& \beta_1 = 0.85 - \dfrac{0.05(f_c^{'} - 28)}{7} \\ f_c^{'} \ge 55, \quad \beta_1 = 0.65 \end{Bmatrix} \tag{4}$$

where ρ_f is the FRP reinforcement ratio, f_f is the tensile strength of FRP bars (MPa), $f_c^{'}$ is the concrete compressive strength (MPa), E_f is the elastic modulus of FRP bars (MPa), ε_{cu} is the concrete ultimate strain (0.003), β_1 is a constant, b is the width of the beam (mm), d is effective depth of the beam (mm), A_f is the area of FRP reinforcement (mm^2), and f_{fu} is the ultimate tensile strength of FRP reinforcement (MPa).

The flexural capacity of under-reinforced FRP-RC beams can be calculated as per Eq. (5):

$$M_n = A_f f_{fu}\left(d - \frac{\beta_1 c_b}{2}\right) \tag{5}$$

$$c_b = \left(\frac{\varepsilon_{cu}}{\varepsilon_{cu} + \quad \varepsilon_{fu}}\right) d \tag{6}$$

where ε_{fu} is the rupture strain of FRP.

2.2. CAN/CSA-S806-12 [16]

According to CAN/CSA-S806–12 [16] design code, the flexural capacity of FRP-RC beam can be calculated as per Eqs. (7) to (11):

$$M_n = \alpha_1\beta_1 f_c^{'} cb\left(d - \frac{\beta_1 c}{2}\right) \tag{7}$$

$$\alpha_1 = 0.85 - 0.0015 f_c^{'} \ge 0.67 \tag{8}$$

$$\beta_1 = 0.97 - 0.0025 f_c^{'} \ge 0.67 \tag{9}$$

$$f_f = \left[\sqrt{\frac{(E_f\varepsilon_{cu})^2}{4} + \frac{\alpha_1\beta_1 f_c^{'}}{\rho_f}E_f\varepsilon_{cu}} - 0.5E_f\varepsilon_{cu}\right] \le f_{fu} \tag{10}$$

$$c = \frac{\rho_f f_f}{\alpha_1\beta_1 f_c^{'}} d \tag{11}$$

where α_1 is a constant and ε_{cu} is 0.0035.

3. Database description

The ML models for predicting the flexural behavior of FRP-RC beams were established using an extensive database of 132 flexural test results reported in the open literature [6,38–59]. The flexural test results were assembled from 24 research articles published between 1991 and 2021. As presented in Table 1 and Fig. 1, six parameters were selected as input parameters, including width and effective depth of the beam, concrete compressive strength, FRP flexural reinforcement ratio, FRP modulus of elasticity, and FRP ultimate tensile strength. Four types of FRP composites were included in the collected database; namely, GFRP, CFRP, BFRP, and AFRP. The beam width and depth, concrete compressive strength, flexural reinforcement ratio, FRP modulus of elasticity, and FRP ultimate strength were in the range of 100–500 mm, 107–512.5 mm, 21–97.4 MPa, 0.12–3.6%, 35.63–147 GPa, and 552–2250 MPa, respectively, as shown in Fig. 1. It should be noted that

Table 1
Geometries and material characteristics of FRP-RC beams included in the database.

References	Number	Geometry		Concrete	Internal reinforcement		
		b_w (mm)	d (mm)	f'_c (MPa)	ρ_f (%)	E_f (MPa)	f_{fu} (MPa)
FAZA and GANGARAO [38]	18	152	216.3-223.8	29-51.71	0.42 - 3.08	48263	896
Benmokrane et al. [49]	9	200	262.5- 512.5	43-52	0.56 - 1.09	42000 - 49000	641 - 689
Duranovic et al. [53]	4	150	210	31.2-43.4	1.36	45000	1000
Almusallam [54]	2	200	157.5-210.7	31.3	1.20-3.60	35630-43370	700-886
Theriault and Benmokrane [55]	12	130	110.6-147.9	46.2-97.4	1.24-3.31	38000	773
Grace et al. [56]	1	152	338	48.3	0.28	147000	2250
Toutanji and Deng [57]	6	180	255-268	35	0.52-1.10	40000	695
Alsayed et al. [58]	4	200	157.5-203.3	31-41	1.15-3.60	35630-43370	700-886
Pecce et al. [59]	2	500	145	30	0.70-1.23	42000	600
Yost et al. [39]	12	191-381	124-192	28	0.12-1.35	41400	830
Wang and Belarbi [40]	3	178	168.5-174.5	48	0.71-3.59	41000-124000	552-2069
Lau and Pam [41]	5	280	359.5-366	33.9-42.5	0.33-1.95	38000-40200	582-603
Kassem et al. [42]	12	200	243.7-245.5	39.1-40.8	0.52-2.08	36000-122000	617-1988
El-Nemr et al. [43]	12	200	297.5-343.5	29-73	0.38-1.95	48700-69300	762-1639
El Refai et al. [44]	3	230	242-244	40	0.40-1.08	50000	1000
Tomlinson and Fam [45]	2	150	270	55.4-57.2	0.14-0.51	70000	1100
Goldston et al. [46]	3	100	124.7-127.8	80	0.49-2.03	37500-55600	732-1764
Alkhraisha et al. [47]	6	180	107-111	30	0.58-2.20	42900-46600	1075-1121
Abed et al. [48]	10	180	182-186	47-70	0.51-1.94	42800-131000	1029-2068
Xiao et al. [50]	1	200	359	21	0.47	50700	901
Abushanab et al. [6]	1	200	260	39.4	0.91	44700	1070
Sun et al. [51]	3	150	210-214	41.6	0.70-1.99	48600-49300	650-680
Sijavandi et al. [52]	1	200	132	37	3.05	46000	1000
Mean		192.1	226.5	44.12	1.24	51565.9	967.7
STD		62.53	87.21	15.75	0.88	22186.9	368.5
Minimum		100	107	21	0.12	35630	552
25%		152	173	33.98	0.58	41000	724
50%		180	222.3	40.6	1.10	46000	891
75%		200	262.5	48.07	1.58	49000	1075
Maximum		500	512.5	97.4	3.6	147000	2250

the cubical compressive strength was converted into cylindrical compressive strength by considering that cylindrical specimens are 80% of the cubical specimens [60]. The established models were trained using a randomly selected 80% of the total database and tested using the remaining 20%.

4. ML model development

In this study, a super-learner model is used to predict the flexural capacity of FRP-RC beams. In addition, the performance of the super-learner model is benchmarked against different widely used boosting- and tree-based models such as classification and regression trees, adaptive boosting, gradient boosted decision trees, and extreme gradient boosting.

4.1. Classification and regression tree

Classification and regression tree (CART) is a supervised ML algorithm that resembles a flowchart-like structure [61]. It is the basis for other powerful ML algorithms. In CART, the most relevant feature is represented in the root node (top node), while each internal node specifies a test on the attribute. The value of the response variable is represented in the leaf nodes, which are used to make a prediction. A tree is built by recursively splitting the input space $\mathbb{R}^N$ into J disjoint feature subspaces $\{R_1, \ldots, R_J\}$ based on a set of splitting rules, where each $R_j \in \mathbb{R}^N$. On each feature subspace R_j, the same prediction is made for all $x \in R_j$. The tree can then be defined as a function $h(x)$, as shown in Eq. (12):

$$h(x) = \sum_{j=0}^{J} b_j I_{(x \epsilon R_j)} \tag{12}$$

where R_j is the j^{th} disjoint region that is assigned to one of the leaves of the tree, b_j is the value of prediction in the region R_j, and $I_{(x \epsilon R_j)}$ is the indicator function that equals unity when $x \in R_j$.

4.2. Adaptive boosting

Boosting algorithms convert weak learners into a single strong learner with reduced bias and variance by combining multiple weak learners a.k.a. base learners sequentially. Adaptive boosting (AdaBoost) was the first successful boosting algorithm. AdaBoost sequentially trains multiple base learners (CARTs in this study) iteratively using reweighted bootstrap samples from the training example to learn the relationship between the input parameters (X) and the response variable (Y). Except for the first iteration, each subsequent base learner is trained from the previous base learner in the sequence by giving more emphasis to incorrectly predicted instances. Consider a training example of N instances in Eq. (13), where (X_i, Y_i) is the i^{th} observation in the training example, X_i is the vector of input parameters, and Y_i is the outcome of interest. The objective of the AdaBoost algorithm is to sequentially train multiple base learners $f_t(X)$ and finally combine them to produce a single strong model F(X), as given in Eq. (14):

$$(\boldsymbol{X}, \boldsymbol{Y}) = \{(X_i, Y_i)\}_{i=1}^{N} \tag{13}$$

$$F(X) = \sum_{t=1}^{T} G\{w_t f_t(X)\} \tag{14}$$

where T is the number of weak learners (CART in this study), w_t is the weight of the t^{th} learner $f_t(X)$, and $G(\cdot)$ is the combination rule.

In the first iteration, the weak learner is trained on the training examples with the uniform distribution with respect to the weights of $\{w_{1,i} = 1/N, \forall i\}$ [62]. In the subsequent iterations, the weights are re-assigned to each observation, with higher weights assigned to incorrectly predicted observations by the previous base learner in the sequence. The weight distribution at iteration step *t* is updated based on Eq. (15), where $\beta_t \in [0, 1]$ is the distribution updating parameter defined by Eq. (16), and $\overline{L_t}$ is the average loss function defined by Eq. (17). In this study, the performance of the base learner is evaluated using linear loss

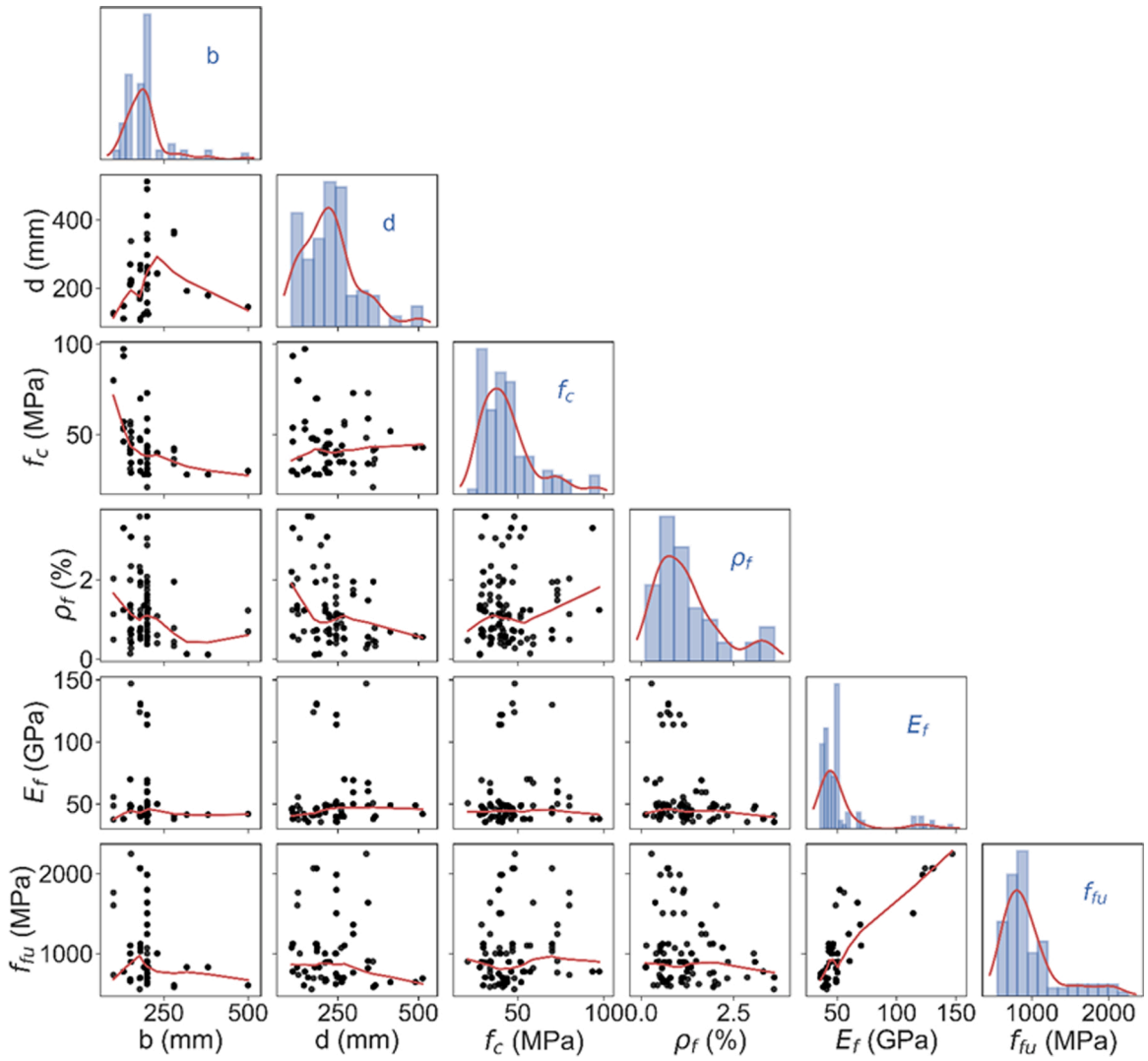

Fig. 1. Statistical distributions of the input and output variables.

function, as given in Eq. (18):

$$w_{t+1,i} = \frac{w_{t,i}\beta_t^{\,1-L_{t,i}}}{\sum_{i=1}^{N} w_{t,i}\beta_t^{\,1-L_{t,i}}} \tag{15}$$

$$\beta_t = \frac{\overline{L_t}}{1-\overline{L_t}} \tag{16}$$

$$\overline{L_t} = \sum_{i=1}^{N} D_{t,i}L_{t,i} \tag{17}$$

$$L_{t,i} = \frac{\left|Y_i - f_{t,i}(X_i)\right|}{max\left|Y_i - f_{t,i}(X_i)\right|}, \quad i = 1, \ldots, N \tag{18}$$

4.3. Gradient boosted decision trees

Similar to other boosting algorithms, the core of gradient boosted decision trees (GBDT) algorithm is to train multiple base learners and accumulate the results of all base learners as the final predicted value of the response variable. The GBDT algorithm uses the gradient descent method to generate new trees based on the previous base learner(s) and minimize the objective function. In the first iteration, the model is initialized with a constant value, as given in Eq. (19). In the subsequent iterations, GBDT fits a new base learner (CART in this study) $h_t(X)$ at each iteration, t as given by Eq. (20), to the negative gradient descent or pseudo-residual ($r_{i,t}$) of the previous learner in the sequence, i.e., training set $\{(x_i, r_{i,t})\}_{i=1}^{N}$, as given by Eq. (21):

$$F_o(X) = \underset{\gamma}{arg\,min} \sum_{i=1}^{N} L(Y_i, \hat{Y}_i) \tag{19}$$

$$F_t(X) = F_{t-1}(X) + \gamma_t h_t(X), \; for\; t = 1, \ldots, T \tag{20}$$

$$r_{i,t} = -\left[\frac{\partial L(Y_i, F(X_i))}{\partial F(X_i)}\right]_{F(X)=F_{t-1}(X)}, \; for\; i = 1, \ldots, N \tag{21}$$

where $L(\cdot)$ is the training loss between the actual (Y) and predicted ($\hat{Y}$) values and γ_t is the multiplier obtained by solving the following one-dimensional optimization problem (Eq. (22)):

$$\gamma_t = \underset{\gamma}{argmin} \sum_{i=1}^{N} L(Y_i, F_{t-1}(X_i) + \gamma h_t(X_i)) \tag{22}$$

4.4. Extreme gradient boosting

Extreme gradient boosting (XGBoost), proposed by Chen and Guestrin [63], is an improvement and extension to gradient boosting.

The objective function in XGBoost comprises a regularization term in addition to the training loss, Eq. (23) [63]:

$$Obj(\theta) = \sum_{i=1}^{N} L(Y_i,\ \widehat{Y}_i) + \sum_{t=1}^{T} \Omega(f_t) \tag{23}$$

Here, $\Omega(\cdot)$ is the regularization term that controls the complexity of the model and prevents overfitting, T is the number of base learners, as defined earlier, and f_t is the model of the t^{th} tree. Generally, the squared error is used for $L(\cdot)$, Eq. (24), while the complexity $\Omega(\cdot)$ is defined by Eq. (25).

$$L(Y_i,\ \widehat{Y}_i) = (Y_i - \widehat{Y}_i)^2 \tag{24}$$

$$\Omega(f_t) = \gamma K + \frac{1}{2}\lambda \|w_t\|^2 \tag{25}$$

where γ and λ are the penalty coefficients, w_t is the leaf weights (scores), and K is the number of leaves in a tree.

Thus, the objective function at step $t \leq T$ can be rewritten as Eq. (26):

$$Obj(t) = \sum_{i=1}^{N} L\left(Y_i,\ \widehat{Y}_{t-1,i} + f_i(X_i)\right) + \Omega(f_t) + constant \tag{26}$$

where $\widehat{Y}_{t-1,i}$ is the predicted value at step $t-1$ and constant term represents $\sum_{k=1}^{t-1}\Omega(f_t)$.

Taking the second-order Taylor expansion of the loss function and removing the high-order infinitesimal terms, the objective function can be given by Eq. (27), where g_i and h_i are the first- and second-order gradients of the loss function.

$$Obj(t) = \sum_{i=1}^{N}\left[L\left(Y_i,\ \widehat{Y}_{t-1,i}\right) + g_i f_t(X_i) + \frac{1}{2}h_i f_t^2(X_i)\right] + \Omega(f_t) + constant \tag{27}$$

$$g_i = \partial_{\widehat{Y}_{t-1,i}} L\left(Y_i,\ \widehat{Y}_{t-1,i}\right) \tag{27a}$$

$$h_i = \partial^2_{\widehat{Y}_{t-1,i}} L\left(Y_i,\ \widehat{Y}_{t-1,i}\right) \tag{27b}$$

Removing all the constants including $L\left(Y_i,\ \widehat{Y}_{t-1,i}\right)$, the objective function can be given by Eq. (28), which can be further simplified as given in Eq. (29) [63]:

$$Obj(t) = \sum_{i=1}^{N}\left[g_i f_t(X_i) + \frac{1}{2}h_i f_t^2(X_i)\right] + \Omega(f_t) \tag{28}$$

$$Obj(t) = \sum_{j=1}^{T}\left[\left(\sum_{i\in I_j} g_i\right)w_j + \frac{1}{2}\left(\sum_{i\in I_j} h_i + \lambda\right)w_j^2\right] + \gamma T \tag{29}$$

where $I_j = \{i|q(x_i) = j\}$ is the set of indices of data points assigned to the j^{th} leaf.

Taking the derivative of the objective function in Eq. (29), the best w_j and the best objective can be given by [63]:

$$w_j^* = -\frac{G_j}{H_j + \lambda} \tag{30}$$

$$Obj^* = -\frac{1}{2}\sum_{j=1}^{T}\frac{G_j^2}{H_j + \lambda} + \gamma T \tag{31}$$

where $G_j = \sum_{i\in I_j} g_i$ and $H_j = \sum_{i\in I_j} h_i$.

4.5. Super-learner model

Super-learner prediction algorithm combines multiple prediction models by assigning different weights to the models to find their optimal combination and produce a single best prediction function [64]. The weights of the candidate learners are estimated through K-fold cross-validation so that the loss function is minimized. The super-learner algorithm maps a training set (X, Y) into a prediction set (Z, Y), in which Z represents the predictions that are constructed using K-fold splits of X. The training process in super-learner model is shown in Fig. 2 and summarized below:

i) Split the training example X into K-folds (K = 10 in this study), as shown in Fig. 2.
ii) Select the base learners: three base models, namely, CART, AdaBoost, and GBDT are used in this study, as shown in Fig. 2.
iii) Perform the following for each base learner (Fig. 2):

- Evaluate the model using K-fold cross-validation.
- Construct a matrix Z by stacking out-of-fold predictions.
- Fit the model on the full training dataset and store the fitted estimator.

i) Fit a meta-model on Z: the meta-model predicts the value of the target variable using Z as input. Linear support vector regression (SVR) is used as a meta-model in this study.

Support vector regression estimates a decision function f(x) in Eq. (32) with a maximum of ε deviation from the value of the target variable for each instance in the training dataset, and at the same time as flat as possible [65]. Given a training dataset $\{(x_1,\ y_1),\ (x_2,\ y_2),\ \ldots,\ (x_N,\ y_N)\}$ with N observations, the aim of SVR is to find a mapping function f(x) given by:

$$f(x) = \omega.\phi(x) + b \tag{32}$$

where $x_i \in \mathbf{X} = \langle x_i^1,\ \ldots,\ x_i^Q\rangle \subseteq \mathbb{R}^Q$, $y_i \in \mathbf{Y} \subseteq \mathbb{R}$, Q is the number of input features, $\phi(x)$ is non-linear mapping, ω is the weight coefficient, and b is the bias.

The optimization problem of Eq. (32) can be transformed into the following by introducing the slack variables ξ_i and ξ_i^*:

$$\underset{w,b,\xi,\xi^*}{min}\ \ \frac{1}{2}\|w\|^2 + C\frac{1}{n}\sum_{i=1}^{n}\left(\xi_i + \xi_i^*\right),\ i = 1,\ 2,\ \ldots,\ N \tag{33}$$

$$\text{Subject to } \left\{\begin{array}{l}(w.\phi(x) + b) - y_i \leq \varepsilon + \xi_i \quad (\xi_i \geq 0)\\ y_i - (w.\phi(x) + b) \leq \varepsilon + \xi_i^* (\xi_i^* \geq 0)\end{array}\right\}.$$

where C is regularization parameter, $\frac{1}{2}\|w\|^2$ is the regular term, ε is the insensitivity function parameter.

The solution of the optimization problem in Eq. (33) is given by [66]:

$$f(x) = \sum_{i\epsilon SV}\left(\alpha_i - \alpha_i'\right)K(x_i,\ x) + b\ subject\ to\ \alpha_i,\ \alpha_i'\ \epsilon\ [0,\ C] \tag{34}$$

here, $K(x_i,\ x)$ is a kernel function, C is a regularization parameter, SV denotes support vectors, which are subsets of training data points, and α_i and α_i' are Lagrange multipliers of the lower and upper support vectors, respectively. The kernel function for linear SVR is given by Eq. (35).

$$k(x, y) = x^T y + constant \tag{35}$$

4.6. Hyperparameter Optimization and performance measures

The database was randomly split into train and test sets in the 80% / 20% proportion, respectively. The training set was used for model training and development, while the test set was used for the final evaluation of the models. Grid search is combined with K-fold cross-validation to optimize the hyperparameters of the ML models. K-fold cross-validation splits the training set into K mutually exclusive and exhaustive sets of as nearly equal size as possible, as shown in Fig. 3 for K = 10. The model is trained on K−1 folds and validated on the

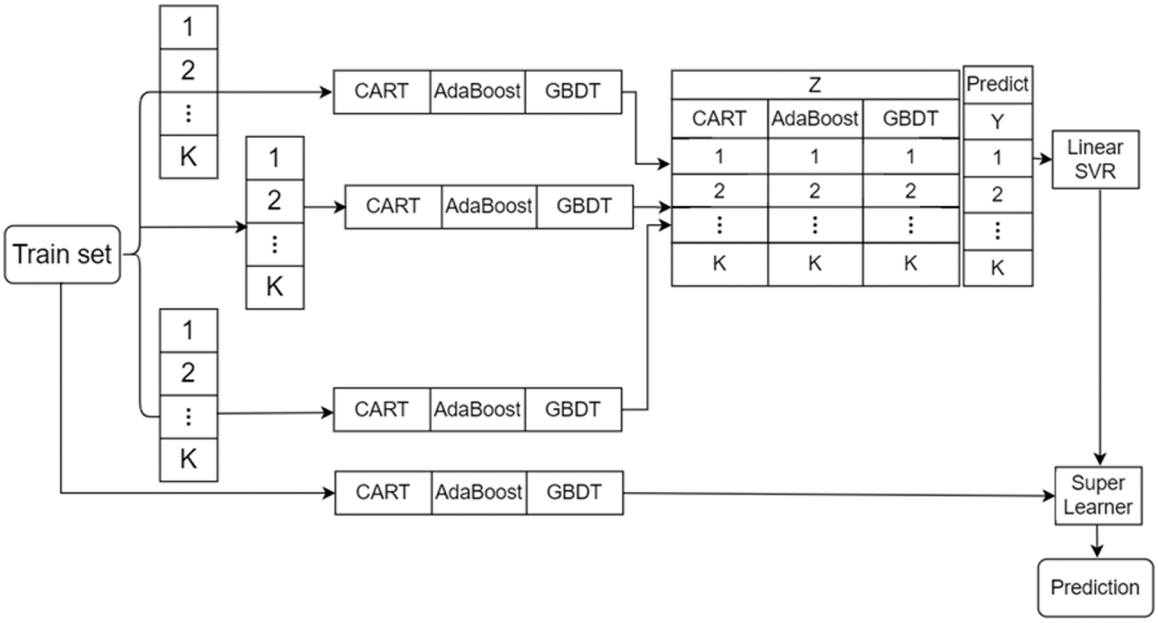

Fig. 2. Training process in super-learner model.

remaining one-fold. This process is repeated K times; thus, each fold and its complement play the role of the validation and training sets, respectively. Finally, the performance of the cross-validated model is taken as the average of the performance from the K validation sets. In this study, a commonly used 10-fold (K = 10) cross-validation is adopted, as shown in Fig. 3.

In addition, commonly used statistical performance metrics such as mean absolute percent error (MAPE), root mean squared error (RMSE), and coefficient of determination (R^2) were used to measure the predictive performance and effectiveness of the developed ML models. The statistical metrics are mathematically expressed in Eqs. (36)–(38), respectively.

- Mean absolute percentage error:

$$MAPE = \frac{1}{N}\sum_{i=1}^{N}\left|\frac{Y_i - \widehat{Y}_i}{Y_i}\right| \quad (36)$$

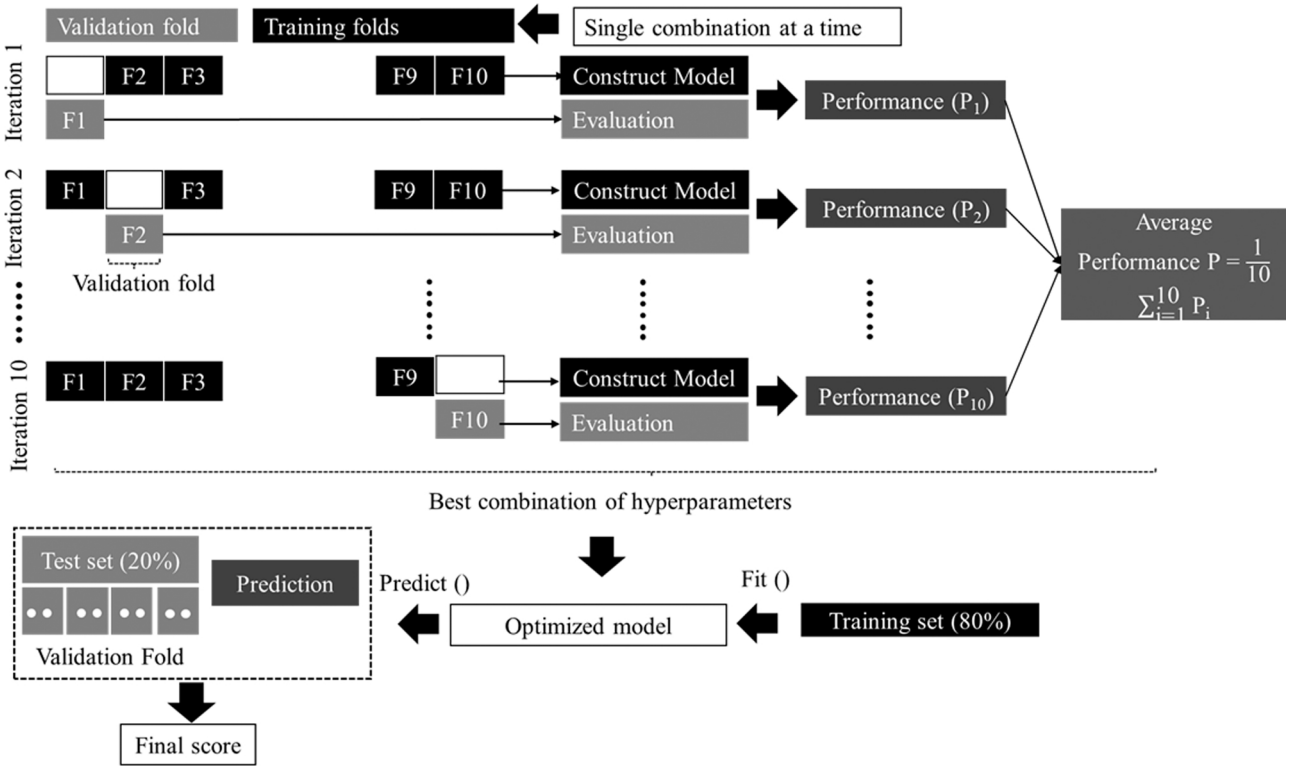

Fig. 3. Hyperparameter optimization using 10-fold cross validation combined with grid search.

- Root mean squared error:

$$RMSE = \sqrt{\frac{1}{N}\sum_{i=1}^{N}(Y_i - \widehat{Y}_i)^2} \quad (37)$$

- Coefficient of determination:

$$R^2 = 1 - \frac{\sum_{i=1}^{N}(Y_i - \widehat{Y}_i)^2}{\sum_{i=1}^{N}(Y_i - \overline{Y})^2} \quad (38)$$

where,

Y_i = experimental flexural capacity,

$\overline{Y}$ = average of the flexural capacity of the beams in the database,

$\widehat{Y}_i$ = predicted flexural capacity, and.

N = number of observations in the database.

The model with the highest R^2 and lowest MAPE and RMSE is considered as the best predictive model. $R^2 = 1$ shows a perfect agreement between the actuals and predictions.

5. Results and discussion

5.1. Optimized ML models and their predictive capabilities

As discussed earlier, a grid search is combined with K-fold cross-validation to optimize the hyperparameters of the ML models using the training set and taking the RMSE as the evaluation index. The optimized hyperparameters for CART include maximum depth of the tree, maximum number of randomly selected input parameters, minimum number of samples required to split an internal node, and minimum number of samples to be at a leaf node. For AdaBoost, the number of estimators (CARTs) and learning rate are optimized in addition to the hyperparameters of its base learner, CART. Similarly, the gradient boosted decision tree is optimized using the number of estimators, learning rate, maximum depth of tree, maximum number of input parameters, minimum number of samples required to split an internal node, and minimum number of samples required to be at a leaf node for base learner. The maximum number of estimators, maximum depth, and learning rate are optimized for XGBoost. The optimal values of the hyperparameters are listed in Table 2 for CART, AdaBoost, GBDT, and XGBoost models. The super-learner model combined the optimized CART, AdaBoost, and GBDT models into a single and strong model using linear SVR as a meta-model.

After optimizing the hyperparameters of each model, their prediction capability is evaluated on the test dataset. Fig. 4a–e show the scatter plots for the experimental moment (M_{exp}) versus predicted moment (M_{pred}) based on the optimized models, in which the abscissa and ordinate show the experimental and predicted flexural capacities, respectively. As shown in these figures, the vast majority of the data points are concentrated on both sides of the equity line ($y = x$), indicating a good agreement between the predicted and experimental flexural capacities. Apart from CART, all models provided predictions within ±20% of the experimental values, as shown in Fig. 4a–e. Fig. 4a–e also provided the coefficient of determination on both the train and test datasets for all models. As can be seen in these figures, the super-learner model provided the highest coefficient of determination on both the train and unseen (test) datasets.

The predictive performance of the ML models is further evaluated based on the previously defined performance metrics and results are presented in Table 3 for both the train and test datasets. As listed in Table 3, the MAPE and RMSE values on the test dataset using the CART model for flexural capacity predictions are the highest at 20.77% and 20.91 kN.m, respectively. All ensemble models showed better prediction accuracy relative to CART, which is logical since ensemble models integrate multiple weak learners to produce a strong learner with a better prediction capability over the base learners. The GBDT and XGBoost models showed comparable prediction performances in predicting the flexural capacities of FRP-RC beams, as shown in Fig. 5 and Table 3. The super-learner model further improved the prediction capability of the models and resulted in the lowest prediction errors: MAPE (6.63%) and RMSE (5.61 kN.m), as well as the highest coefficient of determination of 98.8% on the test dataset, as can be observed in Table 3 and Fig. 5. These results demonstrate the predictive capability of super-learner model amongst other ML models considered in this study.

Table 2
Optimized values of the hyperparameters for different ML models.

Model	Hyperparameter	Optimal value
CART	Maximum depth of the tree	7
	Maximum features	4
	Minimum number of samples required to split an internal node	2
	Minimum number of samples required to be at a leaf node	1
AdaBoost	Base learner	CART
	Maximum number of estimators (CARTs)	85
	Learning rate	0.1
	Maximum of depth of tree for base learner	8
	Maximum features for base learner	4
	Minimum number of samples required to split an internal node for base learner	2
	Minimum number of samples required to be at a leaf node for base learner	1
GBDT	Maximum number of estimators (CARTs)	145
	Maximum depth of tree	3
	Learning rate	0.2
	Maximum features	3
	Minimum number of samples required to split an internal node for base learner	2
	Minimum number of samples required to be at a leaf node for base learner	1
XGBoost	Maximum number of estimators (CARTs)	70
	Maximum depth of tree	3
	Learning rate	0.17

5.2. Comparative study

The flexural capacity of FRP-RC beams estimated using the super-learner model was compared to those predicted using ACI 440.1R-15 [14] and CAN/CSA-S806–12 [16] equations, as shown in Figs. 6 and 7 and Table 4. The comparison was carried out using the statistical measures of R^2, histogram distribution of the predictions, coefficient of variance (COV), MAPE, and RMSE. It can be seen that the predictions of ACI 440.1R-15 [14] were slightly more accurate than CAN/-CSA-S806–12 [16]. As shown in Fig. 6 and Table 4, ACI 440.1R-15 [14] recorded higher R^2 and lower MAPE and RMSE than CAN/CSA-S806–12 [16]. Furthermore, Fig. 7 illustrates that CAN/CSA-S806–12 [16] had a higher variability than ACI 440.1R-15 [14]. The slightly lower accuracy of the CAN/CSA-S806–12 [16] predictions compared to that of ACI 440.1R-15 [14] could be attributed to the fact that CAN/CSA-S806–12 [16] accounts for only over-designed FRP-RC beams, whilst ACI 440.1R-15 [14] considers both over- and under-reinforced FRP-RC beams. Thus, the prediction of the flexural capacity of under-reinforced FRP-RC beams using CAN/CSA-S806–12 [16] design code could be less accurate than that of ACI 440.1R-15 [14]. The scatter plots in Fig. 6 also reveal that many of the predictions obtained by ACI 440.1R-15 [14] and CAN/CSA-S806–12 [16] design code were overestimated, indicating unsafe prediction for the flexural capacity of FRP-RC beams. Moreover, Fig. 6 demonstrates that a considerable number of predictions are over-conservative. Even though over-conservative FRP-RC members ensure that concrete crushing precedes FRP bar rupture, excessive over conservation in FRP-RC beam design requires the use of high amounts of reinforcement, which could increase the manufacturing cost of RC structure and encounter rebar-congestion related problems.

The results depict that the super-learner model outperformed the ACI

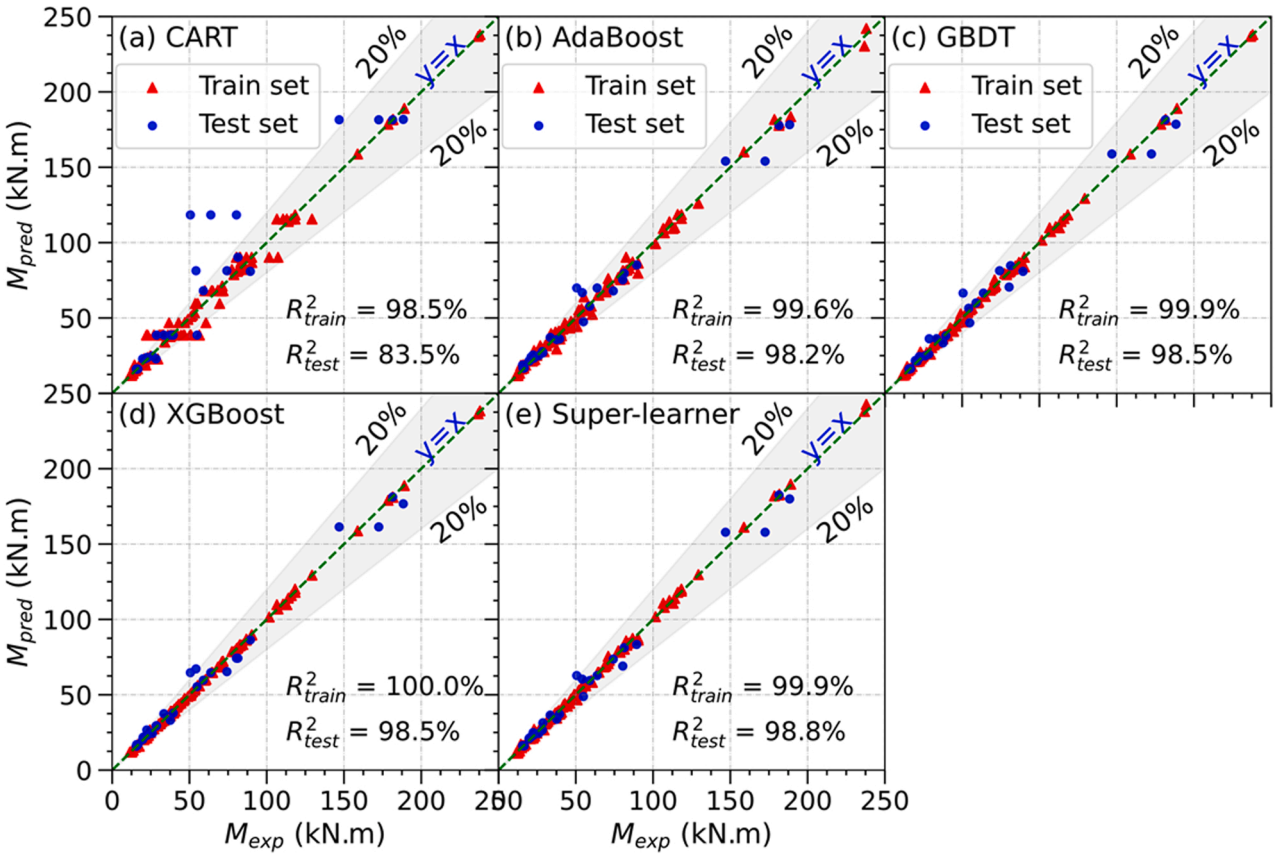

Fig. 4. Experimental versus predicted flexural capacities of FRP-RC beams based on the optimized ML models.

Table 3
Performance metrics of the ML models.

Models	Training set			Test set		
	MAPE (%)	RMSE (kN•m)	R^2 (%)	MAPE (%)	RMSE (kN•m)	R^2 (%)
CART	8.54	5.83	98.5	20.77	20.91	83.5
AdaBoost	4.96	3.10	99.6	8.96	6.91	98.2
GBDT	1.84	1.39	99.9	8.12	6.37	98.5
XGBoost	1.44	0.80	100	7.33	6.33	98.5
Super-learner	1.82	1.61	99.9	6.63	5.61	98.8

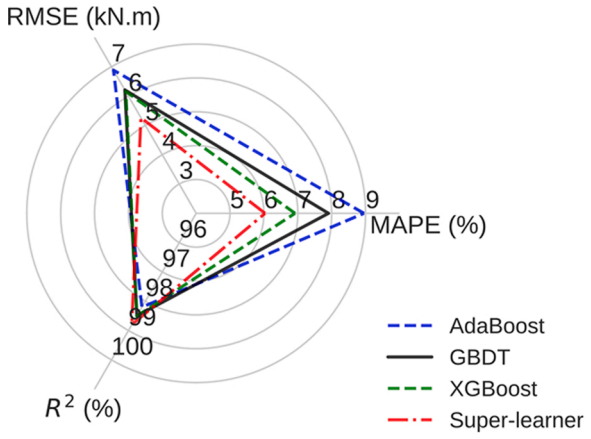

Fig. 5. Predictive performance of boosting ensemble models and super-learner model on the test set.

440.1R-15 [14] and CAN/CSA-S806–12 [16] in estimating the flexural capacity of FRP-RC beams. This could be demonstrated from the scatter plot in Fig. 6, in which most of the predictions by the super-learner model lied within the fitted line, while the predictions of ACI 440.1R-15 [14] and CAN/CSA-S806–12 [16] significantly scattered away from the fitted lines. Additionally, as presented in Table 4, predictions obtained by the super-learner model recorded noticeably higher R^2 and lower MAPE and RMSE than those obtained by 440.1R-15 [14] and CAN/CSA-S806–12 [16]. Moreover, the histogram plotted in Fig. 7 depicts that the variability of the M_{pred}/M_{exp} obtained by the super-learner model results was the closest to 1 among all models. Furthermore, the COV of the super-learner model was 0.05%, whilst ACI 440.1R-15 [14] and CAN/CSA-S806–12 [16] demonstrated COV of 0.3% and 0.34%, respectively. This indicates the adequacy and consistency of the super-learner model in predicting the flexural capacity of FRP-RC beams with different beam geometries, FRP reinforcement types and ratios, and mechanical properties of concrete and FRP composites compared to the standardized equations of ACI 440.1R-15 [14] and CAN/CSA-S806–12 [16].

The performance of the proposed and existing models was further investigated with the use of the Modified Demerits Points Classification (MDPC) method [67] that can be used to evaluate the safety, accuracy, and economic aspects of the predictive models. In this approach, a penalty is assigned to each value of the M_{pred}/M_{exp} ratio based on Table 5. The best predictive model in terms of safety, accuracy, and economic aspects is characterized by the least total penalty based on MDPC method. Fig. 8a–c shows the scatter plots for the M_{pred}/M_{exp} ratio and the number of beams in each region for FRP-RC beams. In these figures, the appropriate safety, conservative, extra conservative, dangerous, and extra dangerous regions are denoted by 'AS', 'C', 'EC', 'D', and 'ED', respectively. As can be observed in Fig. 8a–c, only 41% and 45% of the specimens lied within the appropriate safety region for ACI and CAN/CSA models. By contrast, 97 % of the predictions based on the

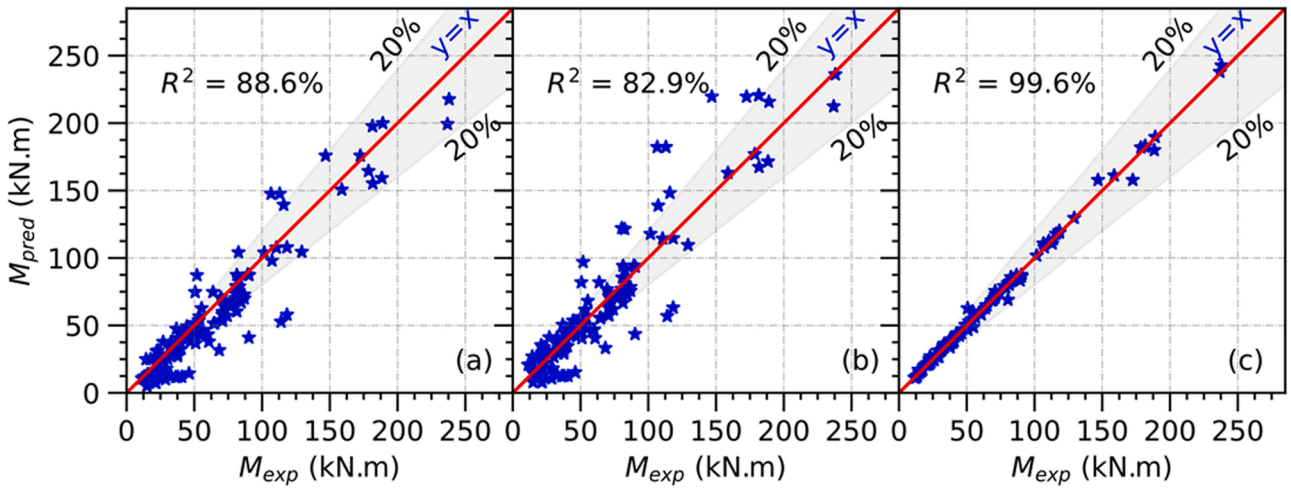

Fig. 6. Experimental versus predicted flexural capacities of FRP-RC beams based on (a) ACI 440.1R-15 [14], (b) CAN/CSA-S806–12 [16], and (c) proposed super-learner models.

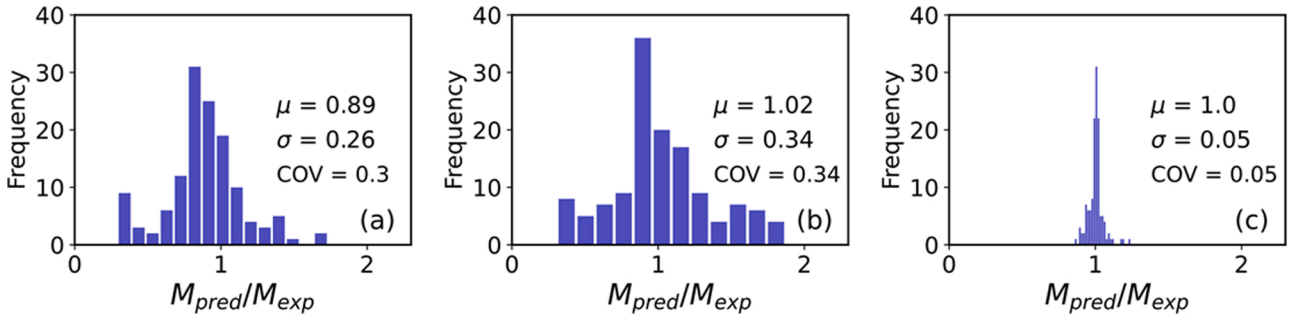

Fig. 7. Histogram of predicted to experimental flexural capacities ratio based on (a) ACI 440.1R-15 [14], (b) CAN/CSA-S806–12 [16], and (c) proposed super-learner models.

Table 4
Performance of existing models and proposed super-learner model on complete dataset.

Model	MAPE (%)	RMSE (kN•m)	R^2 (%)
ACI 440.1R-15[14]	21.81	16.15	88.64
CAN/CSA-S806–12[16]	25.87	19.84	82.85
Super-learner	3.37	2.91	99.63

Table 5
Modified version of the Demerit Points Classification (DPC) criteria [67].

M_{pred}/M_{exp}	Classification	Penalty (PEN)
> 2	Extra dangerous	10
[1.176 – 2]	Dangerous	5
[0.869 – 1.176]	Appropriate safety	0
[0.5 – 0.869]	Conservative	1
≤ 0.5	Extra conservative	2

proposed model lied within the appropriate safety region. In addition, the super-learner model recorded a total penalty of 16, whereas ACI 440.1R-15 [14] and CAN/CSA-S806–12 [16] exhibited a total penalty of 147 and 219, respectively (Table 6). These observations evidenced that the proposed model is superior in predicting the flexural capacity of FRP-RC beams and provided the most accurate, safe, and economic predictions. The superior predictive capability of the proposed ML model is attributed to its capacity to predict the relationship between the predictors and response variable without the need for the prior knowledge of the underlying physical model as opposed to statistical or mathematical approaches that require a predefined set of assumptions.

6. *FAI*: fast, accurate, and intelligent prediction tool

Even though ML models are increasingly used in the field of structural engineering, the practical application of such models is very limited owing to their complex nature. Therefore, practical implementation of such models by providing a user-friendly and efficient tool based on optimized ML models is essential. However, only a few studies provided practical implementation of such models for using them as a predictive tool [68–72]. In this study, a fast, accurate, and intelligent (*FAI*) prediction tool for the flexural capacity of FRP-RC beams is established by deploying the developed super-learner model. The deployed tool can be run on any device, including computers, tablets, and mobile phones. Fig. 9 shows the graphical user interface (GUI) of the developed web-based prediction tool, which can be accessed at: https://frpflexure.herokuapp.com/. As shown in this figure, in the beginning, the user specifies the values of the input parameters, which define the beam geometry, material strength, and internal FRP reinforcement ratio. The summary of the defined values of the input parameters is provided under the summary table in the GUI interface. The flexural capacity of the FRP-RC beams is then automatically computed using the optimized super-learner ML model and displayed under the predicted flexural capacity of the beam section.

7. Conclusion and future work

This study demonstrated the application of ML to develop flexural capacity prediction models for concrete beams reinforced with FRP

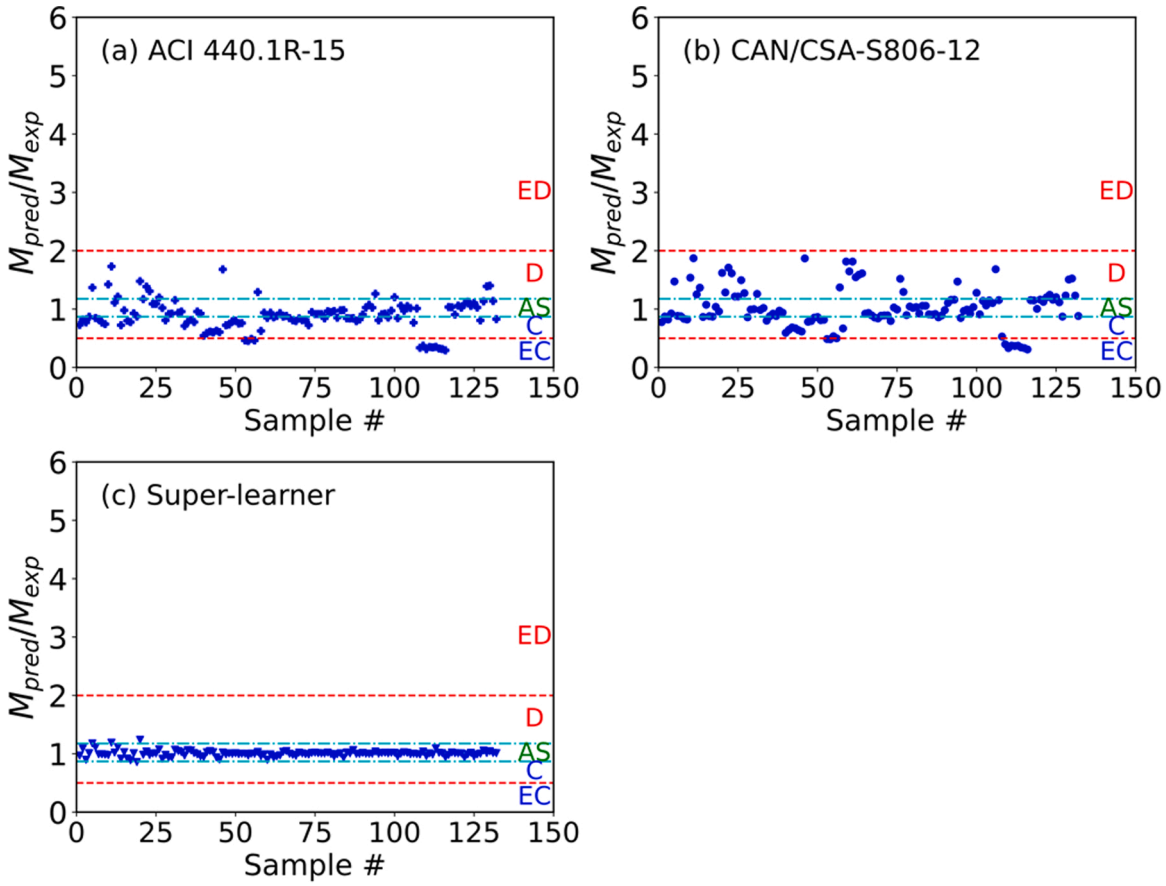

Fig. 8. Flexural capacity prediction capability of the proposed and existing models based on modified DPC [67].

Table 6
Prediction capability of ACI 440.1R-15 [14], CAN/CSA-S806–12 [16], and super-learner models based on modified DPC [67].

Model	Number of specimens					Total penalty
	EC	D	AS	C	EC	
ACI 440.1R-15[14]	0	14	54	51	13	147
CAN/CSA-S806–12[16]	0	34	60	27	11	219
Proposed super-learner	0	3	128	1	0	16

Note: ED, D, AS, C, and EC refer to extra dangerous, dangerous, appropriate safety, conservative, and extra conservative, respectively.

composites. CART and three boosting- and tree-based ensemble models such as AdaBoost, GBDT, and XGBoost were trained and optimized based on a database of FRP-RC beams. A super-learner model was then developed by combining the optimized boosting algorithms using linear support vector regression as a meta-model to develop an accurate, stable, and reliable prediction model for the flexural capacity of FRP-RC beams. The following conclusions can be drawn from this study:

- It is seen that CART has the lowest prediction accuracy for the flexural capacity prediction of FRP-RC beams compared to other considered ML models. The ensemble of CARTs in boosting algorithms including AdaBoost, GBDT, and XGBoost significantly improved the prediction performance of the model.
- All ensemble models performed well in predicting the flexural capacity of FRP-RC beams. The super-learner model outperformed the boosting ensemble algorithms (AdaBoost, GBDT, and XGBoost).
- Among all models investigated in this study, the super-learner model provided the highest predictive performance with the lowest MAPE and RMSE, and highest R^2.
- The comparative analysis showed the superior predictive capability of the proposed model in predicting the flexural capacity of FRP-RC beams over the ACI 440.1R-15 [14] and CAN/CSA-S806-12 [16] equations.
- FAI: fast, accurate, and intelligent prediction tool for the flexural capacity of FRP-RC beams is established by deploying the developed super-learner. The tool can be used for simple and accurate flexural capacity prediction and design of concrete beams reinforced with FRP. The database used in this study was compiled from the open literature that reported experimental results of FRP-RC failed in flexure. With the availability of more experimental results, the developed super-learner-based prediction tool can be updated to improve its generalization ability and range of applicability.

The current study demonstrated the application of different ML models and developed a user-friendly and FAI (Fast, Accurate, and Intelligent) prediction tool for the flexural capacity of FRP-RC beams. Future research is recommended to investigate the use of physics-informed ML models.

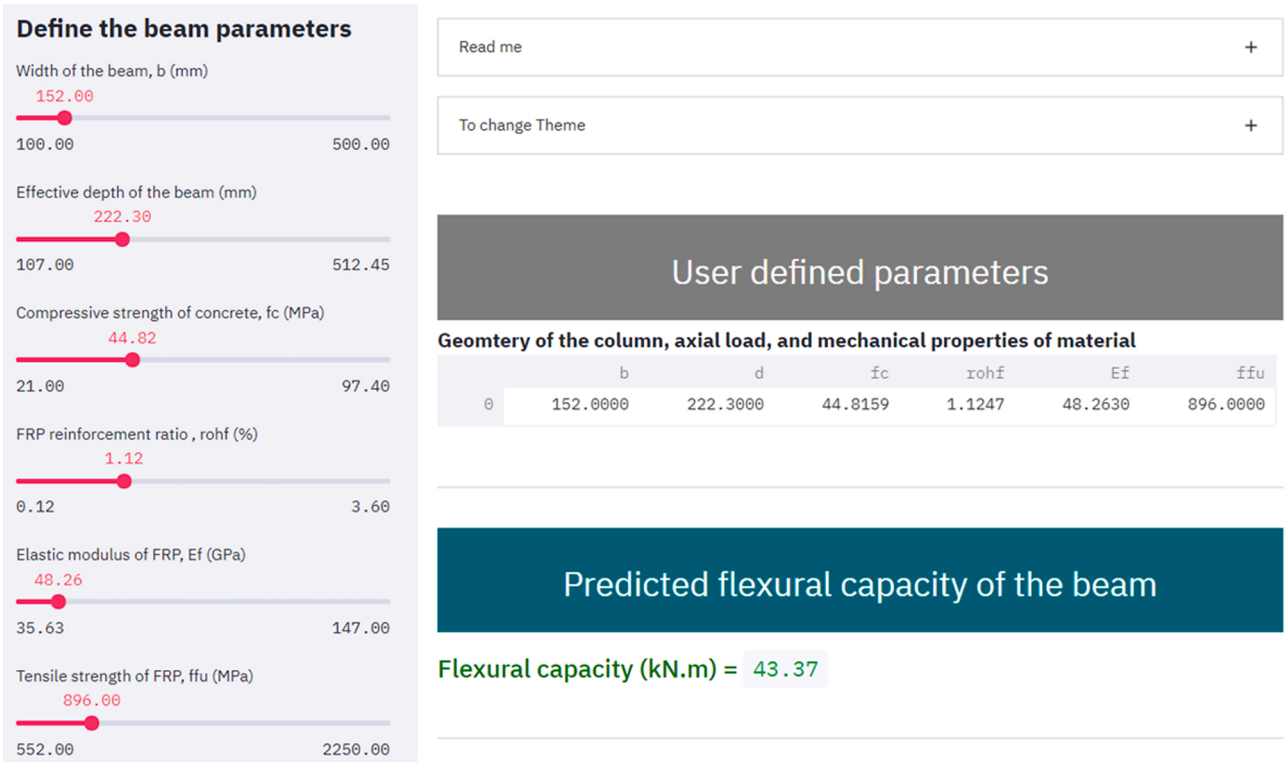

Fig. 9. GUI for predicting the flexural capacity of FRP-RC beams based on the optimized super-learner model.

CRediT authorship contribution statement

Tadesse G. Wakjira: Investigation, Formal analysis, Data curation, Software, Visualization, Conceptualization, Methodology, Validation, Writing – original draft, Writing – review & editing. **Abdelrahman Abushanab:** Investigation, Formal analysis, Data curation, Software, Writing – original draft, Visualization. **Usama Ebead:** Supervision, Project administration, Methodology, Resources, Validation, Writing – review & editing. **Wael Alnahhal:** Conceptualization, Methodology, Validation, Writing – review & editing, Resources, Funding acquisition, Supervision, Project administration.

Declaration of Competing Interest

The authors declare that they have no known competing financial interests or personal relationships that could have appeared to influence the work reported in this paper.

Data Availability

Data will be made available on request.

Acknowledgments

This paper was made possible by NPRP grant # NPRP 13S-0209–200311, UREP award no. UREP21-089-2-039 and GSRA grant no. GSRA6-1-0509-19022 from the Qatar National Research Fund (a member of Qatar Foundation). The findings achieved herein are solely the responsibility of the authors.

References

[1] G.H.H. Koch, M.P.H.P.H. Brongers, N.G.G. Thompson, Y.P.P. Virmani, J.H.H. Payer, Corrosion Cost and Preventive Strategies in the United States [Final report], 2002. ⟨https://rosap.ntl.bts.gov/view/dot/40697⟩.

[2] B. Basaran, Effect of steel–FRP ratio and FRP wrapping layers on tensile properties of glass FRP-wrapped ribbed steel reinforcing bars, Mater. Struct. 54 (2021) 188, https://doi.org/10.1617/s11527-021-01775-x.

[3] A. Abushanab, W. Alnahhal, M. Farraj, Experimental and finite element studies on the structural behavior of BFRC continuous beams reinforced with BFRP bars, Compos. Struct. 281 (2022), 114982, https://doi.org/10.1016/j.compstruct.2021.114982.

[4] M.A. Adam, M. Said, A.A. Mahmoud, A.S. Shanour, Analytical and experimental flexural behavior of concrete beams reinforced with glass fiber reinforced polymers bars, Constr. Build. Mater. 84 (2015) 354–366, https://doi.org/10.1016/j.conbuildmat.2015.03.057.

[5] C.G. Karayannis, P.-M.K. Kosmidou, C.E.E. Chalioris, Reinforced concrete beams with carbon-fiber-reinforced polymer bars—experimental study, Fibers 6 (2018) 99, https://doi.org/10.3390/fib6040099.

[6] A. Abushanab, W. Alnahhal, M. Farraj, Structural performance and moment redistribution of basalt FRC continuous beams reinforced with basalt FRP bars, Eng. Struct. 240 (2021), 112390, https://doi.org/10.1016/j.engstruct.2021.112390.

[7] J. Cheon, M. Lee, M. Kim, Study on the stab resistance mechanism and performance of the carbon, glass and aramid fiber reinforced polymer and hybrid composites, Compos. Struct. 234 (2020), 111690, https://doi.org/10.1016/j.compstruct.2019.111690.

[8] A. Younis, H.E. El-Sherif, U. Ebead, Shear strength of recycled-aggregate concrete beams with glass-FRP stirrups, Compos. Part C Open Access 8 (2022), https://doi.org/10.1016/j.jcomc.2022.100257.

[9] A. Abushanab, W. Alnahhal, Numerical parametric investigation on the moment redistribution of basalt FRC continuous beams with basalt FRP bars, Compos. Struct. 277 (2021), 114618, https://doi.org/10.1016/j.compstruct.2021.114618.

[10] O.I. Abdelkarim, E.A. Ahmed, H.M. Mohamed, B. Benmokrane, Flexural strength and serviceability evaluation of concrete beams reinforced with deformed GFRP bars, Eng. Struct. 186 (2019) 282–296, https://doi.org/10.1016/j.engstruct.2019.02.024.

[11] X. Ruan, C. Lu, K. Xu, G. Xuan, M. Ni, Flexural behavior and serviceability of concrete beams hybrid-reinforced with GFRP bars and steel bars, Compos. Struct. 235 (2020), 111772, https://doi.org/10.1016/j.compstruct.2019.111772.

[12] R.Z. Al-Rousan, M. Alhassan, R. Al-wadi, Nonlinear finite element analysis of full-scale concrete bridge deck slabs reinforced with FRP bars, Structures 27 (2020) 1820–1831, https://doi.org/10.1016/j.istruc.2020.08.024.

[13] A. Abushanab, W. Alnahhal, Performance of basalt fiber reinforced continuous beams with basalt FRP bars, IOP Conf. Ser. Mater. Sci. Eng. 910 (2020), 012004, https://doi.org/10.1088/1757-899X/910/1/012004.

[14] American Concrete Institute (ACI) Committee 440, Guide for the Design and Construction of Structural Concrete Reinforced with Fibre-Reinforced Polymer (FRP) Bars (ACI 440.1R-15), 2015. ⟨https://doi.org/10.1061/40753(171)158⟩.

[15] JSCE (Japan Society of Civil Engineers)., Recommendation for design and construction of concrete structures using continuous fiber reinforcing materials., (1997) 1–58.
[16] CSA (Canadian Standards Association)., Design and construction of building components with fiber reinforced polymers, (CSA-S806–12). (2012).
[17] ISIS (Intelligent Sensing for Innovative Structures)., Reinforcing Concrete Structures with Fibre Reinforced Polymers, 2007.
[18] M. Inel, Modeling ultimate deformation capacity of RC columns using artificial neural networks, Eng. Struct. 29 (2007) 329–335, https://doi.org/10.1016/j.engstruct.2006.05.001.
[19] S. Mangalathu, H. Jang, S.-H. Hwang, J.-S. Jeon, Data-driven machine-learning-based seismic failure mode identification of reinforced concrete shear walls, Eng. Struct. 208 (2020), 110331, https://doi.org/10.1016/j.engstruct.2020.110331.
[20] B. Keshtegar, M.L. Nehdi, N.-T. Trung, R. Kolahchi, Predicting load capacity of shear walls using SVR-RSM model, Appl. Soft Comput. 112 (2021), 107739, https://doi.org/10.1016/j.asoc.2021.107739.
[21] D.-C. Feng, W.-J. Wang, S. Mangalathu, E. Taciroglu, Interpretable XGBoost-SHAP machine-learning model for shear strength prediction of squat RC walls, J. Struct. Eng. 147 (2021), 04021173 https://doi.org/10.1061/(ASCE)ST.1943-541X.0003115.
[22] S. Mangalathu, J.-S. Jeon, Machine learning–based failure mode recognition of circular reinforced concrete bridge columns: comparative study, J. Struct. Eng. 145 (2019) 04019104, https://doi.org/10.1061/(asce)st.1943-541x.0002402.
[23] M.Y. Mansour, M. Dicleli, J.Y. Lee, J. Zhang, Predicting the shear strength of reinforced concrete beams using artificial neural networks, Eng. Struct. 26 (2004) 781–799, https://doi.org/10.1016/j.engstruct.2004.01.011.
[24] J. Amani, R. Moeini, Prediction of shear strength of reinforced concrete beams using adaptive neuro-fuzzy inference system and artificial neural network, Sci. Iran. 19 (2012) 242–248, https://doi.org/10.1016/j.scient.2012.02.009.
[25] J.-S. Chou, T.-P.-T. Pham, T.-K. Nguyen, A.-D. Pham, N.-T. Ngo, Shear strength prediction of reinforced concrete beams by baseline, ensemble, and hybrid machine learning models, Soft Comput. 24 (2020) 3393–3411, https://doi.org/10.1007/s00500-019-04103-2.
[26] J. Chou, N. Ngo, A. Pham, Shear strength prediction in reinforced concrete deep beams using nature-inspired metaheuristic support vector regression, J. Comput. Civ. Eng. 30 (2012) 1–9, https://doi.org/10.1061/(ASCE)CP.1943-5487.0000466.
[27] D.-C. Feng, W.-J. Wang, S. Mangalathu, G. Hu, T. Wu, Implementing ensemble learning methods to predict the shear strength of RC deep beams with/without web reinforcements, Eng. Struct. 235 (2021), 111979, https://doi.org/10.1016/j.engstruct.2021.111979.
[28] B. Fu, D. Feng, A machine learning-based time-dependent shear strength model for corroded reinforced concrete beams, J. Build. Eng. 36 (2021), https://doi.org/10.1016/j.jobe.2020.102118.
[29] T.G. Wakjira, U. Ebead, M.S. Alam, Machine learning-based shear capacity prediction and reliability analysis of shear-critical RC beams strengthened with inorganic composites, Case Stud. Constr. Mater. 16 (2022), e01008, https://doi.org/10.1016/j.cscm.2022.e01008.
[30] T.G. Wakjira, A. Al-Hamrani, U. Ebead, W. Alnahhal, Shear capacity prediction of FRP-RC beams using single and ensenble ExPlainable machine learning models, Compos. Struct. 287 (2022), 115381, https://doi.org/10.1016/j.compstruct.2022.115381.
[31] T.G. Wakjira, M.S. Alam, U. Ebead, Plastic hinge length of rectangular RC columns using ensemble machine learning model, Eng. Struct. 244 (2021), 112808, https://doi.org/10.1016/j.engstruct.2021.112808.
[32] S. Mangalathu, S.H. Hwang, E. Choi, J.S. Jeon, Rapid seismic damage evaluation of bridge portfolios using machine learning techniques, Eng. Struct. 201 (2019), https://doi.org/10.1016/j.engstruct.2019.109785.
[33] S. Mangalathu, H. Sun, C.C. Nweke, Z. Yi, H.V. Burton, Classifying earthquake damage to buildings using machine learning, Earthq. Spectra 36 (2020) 183–208, https://doi.org/10.1177/8755293019878137.
[34] S.H. Hwang, S. Mangalathu, J. Shin, J.S. Jeon, Machine learning-based approaches for seismic demand and collapse of ductile reinforced concrete building frames, J. Build. Eng. 34 (2021), 101905, https://doi.org/10.1016/j.jobe.2020.101905.
[35] S. Mangalathu, J.-S. Jeon, Regional seismic risk assessment of infrastructure systems through machine learning: active learning approach, J. Struct. Eng. 146 (2020), 04020269, https://doi.org/10.1061/(asce)st.1943-541x.0002831.
[36] D. Feng, B. Cetiner, M.R.A. Kakavand, E. Taciroglu, Data-driven approach to predict the plastic hinge length of reinforced concrete columns and its application, J. Struct. Eng. 147 (2021), 04020332, https://doi.org/10.1061/(ASCE)ST.1943-541X.0002852.
[37] A. Ahmad, M. Elchalakani, N. Elmesalami, A. El Refai, F. Abed, Reliability analysis of strength models for short-concrete columns under concentric loading with FRP rebars through artificial neural network, J. Build. Eng. 42 (2021), https://doi.org/10.1016/j.jobe.2021.102497.
[38] S.S. Faza, H.V.S. GANGARAO, Bending and bond behavior and design of concrete beams reinforced with fiber-reinforced plastic rebars, (1991).
[39] J.R. Yost, C.H. Goodspeed, E.R. Schmeckpeper, Flexural performance of concrete beams reinforced with FRP grids, J. Compos. Constr. 5 (2001) 18–25, https://doi.org/10.1061/(ASCE)1090-0268(2001)5:1(18).
[40] H. Wang, A. Belarbi, Flexural behavior of fiber-reinforced-concrete beams reinforced with FRP rebars Acids SP. SP 230 2005.
[41] D. Lau, H.J. Pam, Experimental study of hybrid FRP reinforced concrete beams, Eng. Struct. 32 (2010) 3857–3865, https://doi.org/10.1016/j.engstruct.2010.08.028.
[42] C. Kassem, A.S. Farghaly, B. Benmokrane, Evaluation of flexural behavior and serviceability performance of concrete beams reinforced with FRP bars, J. Compos. Constr. 15 (2011) 682–695, https://doi.org/10.1061/(ASCE)CC.1943-5614.0000216.
[43] A. El-Nemr, E.A. Ahmed, B. Benmokrane, Flexural behavior and serviceability of normal- and high-strength concrete beams reinforced with glass fiber-reinforced polymer bars, Acids Struct. J. 110 (2013), https://doi.org/10.14359/51686162.
[44] A. El Refai, F. Abed, A. Al-Rahmani, Structural performance and serviceability of concrete beams reinforced with hybrid (GFRP and steel) bars, Constr. Build. Mater. 96 (2015) 518–529, https://doi.org/10.1016/j.conbuildmat.2015.08.063.
[45] D. Tomlinson, A. Fam, Performance of concrete beams reinforced with basalt FRP for flexure and shear, J. Compos. Constr. 19 (2015), 04014036, https://doi.org/10.1061/(ASCE)CC.1943-5614.0000491.
[46] M.W. Goldston, A. Remennikov, M.N. Sheikh, Flexural behaviour of GFRP reinforced high strength and ultra high strength concrete beams, Constr. Build. Mater. 131 (2017) 606–617, https://doi.org/10.1016/j.conbuildmat.2016.11.094.
[47] H. Alkhraisha, H. Mhanna, N. Tello, F. Abed, Serviceability and flexural behavior of concrete beams reinforced with basalt fiber-reinforced polymer (BFRP) bars exposed to harsh conditions, Polymers 12 (2020) 2110, https://doi.org/10.3390/polym12092110.
[48] F. Abed, M. Al-Mimar, S. Ahmed, Performance of BFRP RC beams using high strength concrete, Compos. Part C: Open Access 4 (2021), 100107, https://doi.org/10.1016/j.jcomc.2021.100107.
[49] B. Benmokrane, O. Chaallal, R. Masmoudi, Glass fibre reinforced plastic (GFRP) rebars for concrete structures, Constr. Build. Mater. 9 (1995) 353–364, https://doi.org/10.1016/0950-0618(95)00048-8.
[50] S.-H. Xiao, J.-X. Lin, L.-J. Li, Y.-C. Guo, J.-J. Zeng, Z.-H. Xie, F.-F. Wei, M. Li, Experimental study on flexural behavior of concrete beam reinforced with GFRP and steel-fiber composite bars, J. Build. Eng. 43 (2021), 103087, https://doi.org/10.1016/j.jobe.2021.103087.
[51] Q. Sun, Q. Jin, Y. Gao, H. Li, Y. Cao, Flexural behavior of PVA-FRC GFRP reinforced concrete beams, Polym. Compos. 42 (2021) 3331–3348, https://doi.org/10.1002/pc.26062.
[52] K. Sijavandi, M.K. Sharbatdar, A. Kheyroddin, Experimental evaluation of flexural behavior of high-performance fiber reinforced concrete beams using GFRP and high strength steel bars, Structures 33 (2021) 4256–4268, https://doi.org/10.1016/j.istruc.2021.07.020.
[53] N. Duranovic, K. Pilakoutas, P. Waldron, Tests on concrete beams reinforced with glass fibre reinforced plastic bars, Non-Met. Reinf. Concr. Struct. (1997) 479–486.
[54] T.H. Almusallam, Analytical prediction of flexural behavior of concrete beams reinforced by FRP bars, J. Compos. Mater. 31 (1997) 640–657, https://doi.org/10.1177/002199839703100701.
[55] M. Thériault, B. Benmokrane, Effects of FRP reinforcement ratio and concrete strength on flexural behavior of concrete beams, J. Compos. Constr. 2 (1998) 7–16, https://doi.org/10.1061/(ASCE)1090-0268(1998)2:1(7).
[56] N.F. Grace, A.K. Soliman, G. Abdel-Sayed, K.R. Saleh, Behavior and ductility of simple and continuous FRP reinforced beams, J. Compos. Constr. 2 (1998) 186–194, https://doi.org/10.1061/(ASCE)1090-0268(1998)2:4(186).
[57] H. Toutanji, Y. Deng, Deflection and crack-width prediction of concrete beams reinforced with glass FRP rods, Constr. Build. Mater. 17 (2003) 69–74, https://doi.org/10.1016/S0950-0618(02)00094-6.
[58] S. Alsayed, Y. Al-Salloum, T. Almusallam, Performance of glass fiber reinforced plastic bars as a reinforcing material for concrete structures, Compos. Part B Eng. 31 (2000) 555–567, https://doi.org/10.1016/S1359-8368(99)00049-9.
[59] M. Pecce, G. Manfredi, E. Cosenza, Experimental Response and Code Modelsof GFRP RC Beams in Bending, J. Compos. Constr. 4 (2000) 182–190, https://doi.org/10.1061/(ASCE)1090-0268(2000)4:4(182).
[60] British Standards Institution, Concrete–complementary British Standard to BS EN 206–1: Specification for Constituent Materials and Concrete, BSI, 2006.
[61] C.D. Sutton, Classification and regression trees, bagging, and boosting, Handb. Stat. 24 (2005) 303–329, https://doi.org/10.1016/S0169-7161(04)24011-1.
[62] D.L. Shrestha, D.P. Solomatine, Experiments with AdaBoost.RT: an improved boosting scheme for regression, Neural Comput. 18 (2006) 1678–1710, https://doi.org/10.1162/neco.2006.18.7.1678.
[63] T. Chen, C. Guestrin, Xgboost: A scalable tree boosting system 22nd SIGKDD Conf. Knowl. Discov. Data Min. 2016.
[64] M.J. Van Der Laan, E.C. Polley, A.E. Hubbard, Super learner, Stat. Appl. Genet. Mol. Biol. 6 (2007), https://doi.org/10.2202/1544-6115.1309.
[65] B. Dong, C. Cao, S.E. Lee, Applying support vector machines to predict building energy consumption in tropical region, Energy Build. 37 (2005) 545–553, https://doi.org/10.1016/j.enbuild.2004.09.009.
[66] H. Yu, S. Kim, SVM tutorial-classification, regression and ranking, Handb. Nat. Comput. 4 (2012) 479–506, https://doi.org/10.1007/978-3-540-92910-9_15.

[67] B.N.M. Neto, J.A.O. Barros, G.S.S.A. Melo, Model to Simulate the Contribution of Fiber Reinforcement for the Punching Resistance of RC Slabs, J. Mater. Civ. Eng. 26 (2014) 04014020, https://doi.org/10.1061/(ASCE)MT.1943-5533.
[68] M.Z. Naser, H. Salehi, Machine learning-driven assessment of fire-induced concrete spalling of columns, Acids Mater. J. 117 (2020) 7–16, https://doi.org/10.14359/51728120.
[69] M. Abedi, M.Z. Naser, RAI: rapid, Autonomous and Intelligent machine learning approach to identify fire-vulnerable bridges, Appl. Soft Comput. 113 (2021), 107896, https://doi.org/10.1016/j.asoc.2021.107896.
[70] A.S. Bakouregui, H.M. Mohamed, A. Yahia, B. Benmokrane, Explainable extreme gradient boosting tree-based prediction of load-carrying capacity of FRP-RC columns, Eng. Struct. 245 (2021), 112836, https://doi.org/10.1016/j.engstruct.2021.112836.
[71] T.G. Wakjira, M. Ibrahim, U. Ebead, M.S. Alam, Explainable machine learning model and reliability analysis for flexural capacity prediction of RC beams strengthened in flexure with FRCM, Eng. Struct. 255 (2022), https://doi.org/10.1016/j.engstruct.2022.113903.
[72] T.G. Wakjira, A. Rahmzadeh, M.S. Alam, R. Tremblay, Explainable machine learning based efficient prediction tool for lateral cyclic response of post-tensioned base rocking steel bridge piers, Structures 44 (2022) 947–964, https://doi.org/10.1016/j.istruc.2022.08.023.